Nonsequential double ionization of helium in IR+XUV two-color laser fields: Collision-ionization process

Facheng Jin,[1] Yuanye Tian,[1,2] Jing Chen,[3] Yujun Yang,[2] Xiaojun Liu,[4] Zong-Chao Yan,[5] and Bingbing Wang[1,*]

[1]*Laboratory of Optical Physics, Beijing National Laboratory for Condensed Matter Physics, Institute of Physics, Chinese Academy of Sciences, Beijing 100190, China*

[2]*Institute of Atomic and Molecular Physics, Jilin University, Changchun 130012, China*

[3]*Institute of Applied Physics and Computational Mathematics, P.O. Box 8009, Beijing 100088, China*

[4]*State Key Laboratory of Magnetic Resonance and Atomic and Molecular Physics, Wuhan Institute of Physics and Mathematics, Chinese Academy of Sciences, Wuhan 430071, China*

[5]*Department of Physics, University of New Brunswick, Fredericton, New Brunswick, Canada E3B 5A3*

(Received 14 October 2015; revised manuscript received 26 November 2015; published 21 April 2016)

We investigate the nonsequential double ionization (NSDI) process of an atom in IR+XUV two-color intense laser fields, where the photon energy of the XUV laser is higher than the atomic ionization threshold. By using the frequency-domain theory, we consider the NSDI as a process caused by the collision-ionization mechanism and obtain the NSDI spectrum that presents a multiplateau structure. With the help of channel analysis, we find that the height of a plateau in the NSDI spectrum is determined by the number of XUV photons absorbed by the electrons. Furthermore, to explain the interference structure in the NSDI spectrum, we also compare the contributions of forward and backward collisions to the NSDI probability. We find that the forward collision dominates the contributions to the NSDI when two electrons are ejected along the same direction and both forward and backward collisions make a comparable contribution to NSDI when the two electrons are ejected along opposite directions. By applying the saddle-point approximation, we obtain an energy-circle formula, which may illustrate the formation of the NSDI spectrum structure.

DOI: 10.1103/PhysRevA.93.043417

I. INTRODUCTION

Two-color laser fields have become effective tools for studying extreme nonlinear strong-field phenomena, such as above-threshold ionization (ATI) [1,2], high-order harmonic generation (HHG) [1–12], and nonsequential double ionization (NSDI) [13,14]. On the one hand, when photon energies of two-color laser fields are much smaller than the atomic ionization threshold, we can regard the two laser fields as classical fields and hence optimizing the conditions of the two-color laser fields may change the recollision electron's trajectories, leading to a change of ionization or emission spectrum. For example, controlling the time delay between two laser fields can greatly widen the spectra of ATI [1] and HHG [11]. On the other hand, when one laser photon energy in the two-color laser fields is close to or higher than the atomic ionization threshold, i.e., one frequency is in the extreme ultraviolet (XUV) regime, one may consider this high-frequency laser as a quantized field instead of a classical one. Therefore, the high-frequency laser field may play a different role in the interaction between atoms and IR+XUV two-color laser fields. For example, it has been found that the photoelectron spectra present a plateau or sideband structure in the IR+XUV two-color laser fields [15–18], where the XUV laser field ionizes an electron by a multiphoton transition.

The NSDI in an intense IR laser field has continuously attracted much attention since its first experimental observation of Xe [19]. The experimental NSDI results display a knee structure of the ion-count data as a function of the laser intensity because of the electron-electron correlations [20]. It was later found that the ion momentum distributions of NSDI processes show a double-hump or single-hump structure [21–24]. Up to now, the widely accepted mechanism of NSDI in an IR laser field has been the recollision model [25,26]. This recollision mechanism can be classified into two types: a collision-ionization (CI) mechanism and a collision-excitation-ionization (CEI) mechanism, which depends on the conditions of the atom-laser system [24,27]. Many investigations have explicitly shown that the probability of an NSDI process due to the CI mechanism is dominated by the two ionized electrons with their momenta along the same direction [23,28], while the probability caused by the CEI mechanism is expected to be found with the two ionized electrons emitted in any direction [24,29]. Furthermore, it is found that the NSDI can also take place in an XUV laser field [30–39]. For the one-photon double ionization, this process has been well understood [30,31] after many years of extensive studies. Recently, two-photon double ionization processes have been investigated in experiments because of the development of the XUV attosecond sources [32–34]. Moreover, many theoretical methods have also focused on dealing with the two-photon double ionization processes [35], including two-photon sequential double ionization and NSDI. Although it remains unclear how to quantitatively distinguish and characterize sequential and nonsequential contributions [36], the character of the momentum distributions for the two electrons can be directly identified [37]. It has been demonstrated that the momentum distribution of double ionization in an XUV laser field strongly depends on the XUV photon energy and the laser duration [37,38], where the momentum distribution can be shown on a certain energy circle in the NSDI process [37,39]. From previous studies we can see that

*wbb@aphy.iphy.ac.cn

 ©2016 American Physical Society

the momentum spectrum is an appropriate tool for studying the NSDI processes both experimentally and theoretically [26,28]. Despite the enormous progress that has been made in the past in studying NSDI [26,35], there have been only a few investigations of the double ionization in IR+XUV two-color laser fields. Recently, Hu [40] calculated the double ionization of helium in IR+XUV two-color laser fields by the full-dimensional *ab initio* method. It was shown that the double ionization probability can be extremely enhanced by attosecond control of the electron correlation. More recently, Liu and Thumm [41,42] calculated the joint angular distribution in the laser-assisted XUV double ionization of helium. It was found that the IR laser field enhances side-by-side and enables back-to-back emission and also facilitates the formation of a sideband pattern in the energy distribution, which is totally different from the case of a monochromatic XUV or IR laser field. The present investigation focuses on the momentum spectrum of the NSDI process in IR+ XUV two-color laser fields.

With the help of formal scattering theory [43], the frequency-domain theory based on the nonperturbative quantum electrodynamics was first developed by Guo and Drake [44]. In this frequency-domain theory, all dynamic processes can be naturally regarded as quantum transitions in one isolated laser-matter system, where the laser field, as part of the whole system, is treated as a quantized field. This approach has been extended to deal with recollision processes [45–52], including HHG, high-order above-threshold ionization (HATI), and NSDI. In contrast with the advantage of the conventional nonstationary perturbation theory to study the electron trajectories and provide the cutoff law of recollision processes [48], the advantage of the frequency-domain theory can be classified into three aspects: (i) all recollision processes can be decoupled into a direct ATI followed by a laser-assisted collision (LAC) or laser-assisted recombination so that one can investigate the role of these subprocesses separately; (ii) this approach can save a large amount of computation time because of its time-independent characteristic; (iii) all of the recollision processes, including HHG, HATI, and NSDI, can be dealt with under a unified theoretical frame, where the relationship among all these recollision processes can be investigated conveniently [46,48,52]. Recently, the frequency-domain theory has been employed to study the dependence of the ATI spectrum on IR and XUV two-color laser fields and it was found that two-color laser fields play different roles for the ATI spectrum [15,53]. According to the frequency-domain theory, the NSDI process caused by the CI mechanism can be treated as a two-step process [52]: an ATI followed by an LAC. Wang *et al.* [52] have investigated the contribution of the NSDI momentum spectrum in an IR laser field, where the NSDI probability is dominated by the two ionized electrons along the same direction and the backward collision makes a major contribution to the NSDI probability. In this work we investigate the NSDI process in IR+XUV two-color laser fields. We find that the NSDI momentum spectra show a multiplateau structure. By analyzing the channel contributions, we find that the XUV photon number absorbed by the electrons determines the height of a plateau and the interference between trajectories in each channel forms the structure of a plateau in the NSDI spectrum.

II. THEORETICAL METHOD

The Hamiltonian for a two-electron atom exposed to a two-color linearly polarized laser field of frequencies ω_1 and ω_2 is (atomic units are used throughout unless otherwise stated) [44]

$$H = H_0 + U + V, \tag{1}$$

where

$$H_0 = \frac{(-i\nabla_1)^2}{2} + \frac{(-i\nabla_2)^2}{2} + \omega_1 N_{a1} + \omega_2 N_{a2} \tag{2}$$

is the energy operator for the laser-matter system. Here N_{ai} is the photon number operator for the laser field of frequency ω_i with $i = 1,2$. In addition, $U = U_1 + U_2 + U_{12}$, where U_1 and U_2 are the interaction potentials between each electrons and nucleus, respectively, and U_{12} is the interaction potential between the two electrons. Finally, the electron-photon interaction potential is $V = V_1 + V_2$, where

$$V_j = -[(-i\nabla_j)\cdot\mathbf{A}_1(-\mathbf{k}_1\cdot\mathbf{r}_j) + (-i\nabla_j)\cdot\mathbf{A}_2(-\mathbf{k}_2\cdot\mathbf{r}_j)] + \tfrac{1}{2}[\mathbf{A}_1(-\mathbf{k}_1\cdot\mathbf{r}_j) + \mathbf{A}_2(-\mathbf{k}_2\cdot\mathbf{r}_j)]^2, \tag{3}$$

with $\mathbf{A}_s(-\mathbf{k}_s\cdot\mathbf{r}_j) = (2V_{\gamma_s}\omega_s)^{-1/2}(\hat{\varepsilon}_s e^{i\mathbf{k}_s\cdot\mathbf{r}_j}a_s + \text{c.c.})$ ($s = 1,2$ and $j = 1,2$) the vector potential, $\mathbf{k}_s$ the wave vector, $\hat{\varepsilon}_s$ the polarization vector, a_s ($a_s^\dagger$) the annihilation (creation) operator, and V_{γ_s} the normalization volume of the laser field of frequency ω_s.

The transition matrix from the initial state $|\Psi_i\rangle$ to the final state $|\Psi_f\rangle$ for an NSDI process due to the CI mechanism is [52]

$$T_{\mathrm{CI}} = \langle\Psi_f|U_{12}\frac{1}{E_i - H + i\varepsilon}V_1|\Psi_i\rangle. \tag{4}$$

Here $|\Psi_i\rangle = |\Psi_{in_1n_2}(\mathbf{r}_1,\mathbf{r}_2)\rangle = |\Phi_1(\mathbf{r}_1,\mathbf{r}_2)\rangle\otimes|n_1\rangle\otimes|n_2\rangle$, where $|\Phi_1(\mathbf{r}_1,\mathbf{r}_2)\rangle$ is the ground state of the atom, $|n_j\rangle$ is the Fock state of the laser field with the photon number n_j for $j = 1,2$, and E_i is the total energy of the system in the initial state $E_i = -(I_{p_1} + I_{p_2}) + (n_1 + 1/2)\omega_1 + (n_2 + 1/2)\omega_2$, with I_{p_1} (I_{p_2}) being the first (second) ionization potential of the atom. The final state is $|\Psi_f\rangle = |\Psi_{\mathbf{p}_1\mathbf{p}_2k_1k_2}(\mathbf{r}_1,\mathbf{r}_2)\rangle$ with the energy $E_j = \mathbf{p}_1^2/2 + \mathbf{p}_2^2/2 + (k_1 + 1/2)\omega_1 + (k_2 + 1/2)\omega_2 + 2u_{p_1}\omega_1 + 2u_{p_2}\omega_2$, where $u_{p_1} = U_{p_1}/\omega_1$ and $u_{p_2} = U_{p_2}/\omega_2$ with U_{p_1} (U_{p_2}) being the ponderomotive energy of the first (second) laser field, and $|\Psi_{\mathbf{p}_1\mathbf{p}_2k_1k_2}(\mathbf{r}_1,\mathbf{r}_2)\rangle$ is the quantized-field Volkov state of two electrons in a two-color laser field [44,52]

$$|\Psi_{\mathbf{p}_1\mathbf{p}_2k_1k_2}(\mathbf{r}_1,\mathbf{r}_2)\rangle = V_e^{-1}\exp\{i[(\mathbf{p}_1 + u_{p_1}\mathbf{k}_1 + u_{p_2}\mathbf{k}_2)\cdot\mathbf{r}_1 + (\mathbf{p}_2 + u_{p_1}\mathbf{k}_1 + u_{p_2}\mathbf{k}_2)\cdot\mathbf{r}_2]\} \times \sum_{j_1=-k_1,j_2=-k_2}^{\infty}\aleph_{j_1j_2}(\zeta_1)^*\exp\{-i[j_1(\mathbf{k}_1\cdot\mathbf{r}_1 + \phi_1) + j_2(\mathbf{k}_2\cdot\mathbf{r}_1 + \phi_2)]\}$$

$$\times \sum_{j_3=-k_1-j_1,\, j_4=-k_2-j_2}^{\infty} \aleph_{j_3 j_4}(\zeta_2)^* \exp\{-i[j_3(\mathbf{k}_1\cdot\mathbf{r}_2+\phi_1)+j_4(\mathbf{k}_2\cdot\mathbf{r}_2+\phi_2)]\}$$
$$\times|k_1+j_1+j_3,k_2+j_2+j_4\rangle, \tag{5}$$

with ϕ_1 and ϕ_2 being the initial phases of the two-color laser fields, respectively. We should note that the interaction between the two ionized electrons is ignored in the final state (5). The terms $\aleph_{j_1 j_2}(\zeta_1)$ and $\aleph_{j_3 j_4}(\zeta_2)$ in Eq. (5) are the generalized Bessel functions, which can be written as [44]

$$\aleph_{q_1 q_2}(\varsigma) = \sum_{q_3 q_4 q_5 q_6} J_{-q_1+2q_3+q_5+q_6}(\varsigma_1) J_{-q_2+2q_4+q_5-q_6}(\varsigma_2) \times J_{-q_3}(\varsigma_3) J_{-q_4}(\varsigma_4) J_{-q_5}(\varsigma_5) J_{-q_6}(\varsigma_6), \tag{6}$$

where

$$\varsigma_1 = 2\sqrt{\frac{u_{p_1}}{\omega_1}}|\mathbf{p}_i\cdot\hat{\epsilon}_1|, \quad \varsigma_2 = 2\sqrt{\frac{u_{p_2}}{\omega_2}}|\mathbf{p}_i\cdot\hat{\epsilon}_2|,$$
$$\varsigma_3 = \frac{1}{2}u_{p_1}, \quad \varsigma_4 = \frac{1}{2}u_{p_2}, \tag{7}$$
$$\varsigma_5 = 2\frac{\sqrt{u_{p_1}\omega_1 u_{p_2}\omega_2}}{\omega_1+\omega_2}, \quad \varsigma_6 = 2\frac{\sqrt{u_{p_1}\omega_1 u_{p_2}\omega_2}}{\omega_1-\omega_2},$$

and $J_m(t)$ is the Bessel function of order m. In above expressions, $\mathbf{p}_i$ $(i=1,2)$ is the momentum of the ionized electron.

In the NSDI process, an intermediate state including one electron ionized and the other electron still bounded can be expressed as $|\Psi_{\mathbf{p}_1 m_1 m_2}(\mathbf{r}_1)\rangle \otimes |\Phi_1(\mathbf{r}_2)\rangle$, where $|\Phi_1(\mathbf{r}_2)\rangle$ is the ground state of He^+ and $|\Psi_{\mathbf{p}_1 m_1 m_2}(\mathbf{r}_1)\rangle$ is the Volkov state, which can be written as [44]

$$|\Psi_{\mathbf{p}_1 m_1 m_2}(\mathbf{r}_1)\rangle = V_e^{-1/2} \sum_{j_1=-m_1,\, j_2=-m_2}^{\infty} \exp\{i[\mathbf{p}_1+(u_{p_1}-j_1)\times\mathbf{k}_1+(u_{p_2}-j_2)\mathbf{k}_2]\cdot\mathbf{r}_1\} \times \aleph_{j_1 j_2}(\zeta_1)^* \exp[-i(j_1\phi_1+j_2\phi_2)] \times |m_1+j_1, m_2+j_2\rangle, \tag{8}$$

with the energy $E_m = \mathbf{p}_1^2/2 + (m_1+1/2)\omega_1 + (m_2+1/2)\omega_2 + U_{p1} + U_{p2}$. Here $\mathbf{p}_1$ is the momentum of ionized electron, m_i is the number of photons in the occupation number representation, and j_i is the photon number transferred between the laser field and one of electrons, with $i=1$ or 2.

By applying the completeness relation of the intermediate states with the assumption that the bound electron is in the ground state of the He^+ ion, Eq. (4) can be rewritten as

$$T_{\mathrm{CI}} = -i\pi \sum_{\mathbf{p}_1' m_1 m_2}^{\infty} \langle\Psi_{\mathbf{p}_1\mathbf{p}_2 k_1 k_2}(\mathbf{r}_1,\mathbf{r}_2)|U_{12}|\Psi_{\mathbf{p}_1' m_1 m_2}(\mathbf{r}_1)\Phi_1(\mathbf{r}_2)\rangle \times \langle\Psi_{\mathbf{p}_1' m_1 m_2}(\mathbf{r}_1)\Phi_1(\mathbf{r}_2)| \times V_1|\Psi_{i n_1 n_2}(\mathbf{r}_1,\mathbf{r}_2)\rangle\delta(E_{\mathbf{p}_1' m_1 m_2} - E_i), \tag{9}$$

where $E_{\mathbf{p}_1' m_1 m_2}$ is the corresponding energy of an intermediate state. We notice that the term $\langle\Psi_{\mathbf{p}_1' m_1 m_2}(\mathbf{r}_1)\Phi_1(\mathbf{r}_2)| V_1|\Psi_{i n_1 n_2}(\mathbf{r}_1,\mathbf{r}_2)\rangle$ represents the ATI process, where an electron is ionized directly by a two-color laser field, and the term $\langle\Psi_{\mathbf{p}_1\mathbf{p}_2 k_1 k_2}(\mathbf{r}_1,\mathbf{r}_2)|U_{12}|\Psi_{\mathbf{p}_1' m_1 m_2}(\mathbf{r}_1)\Phi_1(\mathbf{r}_2)\rangle$ represents the LAC process, where the first ionized electron collides with the bound electron and sets it free from the bound state. By using Eqs. (5) and (8), the transition matrix for the NSDI can be written as

$$T_{\mathrm{CI}} = -4i\pi^2 V_e^{-2} \sum_{s_1 s_2} I(\mathbf{P})\aleph_{q_1 q_2}(\zeta_1+\zeta_2-\zeta_1') \times [(u_{p_1}-s_1)\omega_1 + (u_{p_2}-s_2)\omega_2]\aleph_{s_1 s_2}(\zeta_1')\Phi_1(\mathbf{p}_1'), \tag{10}$$

where

$$I(\mathbf{P}) = \int\int d\mathbf{r}_1 d\mathbf{r}_2 \exp[-i(\mathbf{p}_1-\mathbf{p}_1')\cdot\mathbf{r}_1] \times \exp(-i\mathbf{p}_2\cdot\mathbf{r}_2)U_{12}\Phi_1(\mathbf{r}_2). \tag{11}$$

In the above, $s_1 = n_1 - m_1$ and $s_2 = n_2 - m_2$ are the photon numbers absorbed from the first and second laser fields in the ATI process, $q_1 = m_1 - k_1$ and $q_2 = m_2 - k_2$ are the photon numbers absorbed from the first and second laser fields in the LAC process, and $\mathbf{p}_1'$ is the momentum of the ionized electron in the ATI process.

III. NUMERICAL RESULTS

A. The NSDI momentum spectrum and channel analysis

We now consider the NSDI of helium in an IR+XUV two-color laser field through the collision-ionization process. The atomic double-ionization threshold of helium is $I_p = 79.0$ eV and the frequencies of the two laser fields are $\omega_1 = 1.165$ eV and $\omega_2 = 75\omega_1$. The intensities of the IR and XUV lasers are $I_1 = I_2 = 3.6\times10^{13}$ W cm^{-2}, the polarization directions of the two-color laser fields are the same, and the initial phases of the two laser fields are set equal to zero. In our calculation, the ranges of absorbing photon numbers in units of IR photon are $25 \leqslant s_1+s_2 \leqslant 135$ and $75 \leqslant s_1+s_2+q_1+q_2 \leqslant 260$, where the maximum numbers of IR and XUV photons make the calculation results convergent. The minimum photon numbers 25 and 75 are determined by the ionization thresholds in the ATI and NSDI processes, respectively. In order to save computer time, we use the photon energy of the IR laser as an interval of energy in our calculation, hence the interval of momentum is $\triangle p = \sqrt{2\hbar\omega_1} = 0.34$. Therefore, the value of the momentum in the figures, which is smaller than 0.34, may be missed. Specifically, the formula of breakpoint sequence is $p_j = \sqrt{2(E_j - I_{p_j} - U_{p_1} - U_{p_2})}$ with E_j being the absorbing photon energy and I_{p_j} being ionization potential as well as U_{p_1}, U_{p_2} being the ponderomotive energy with $j=1,2$. It should be noted that the absorbing photon energy E_j is in units of the IR photon, which leads to the lack of continuity at the quadrant boundaries in our figures. If the interval of the energy is decreased, the momentum spectrum may be continuous at the quadrant boundaries. Figure 1 shows the NSDI momentum spectra of two ionized electrons with their momenta parallel to the lasers polarization directions. This result qualitatively

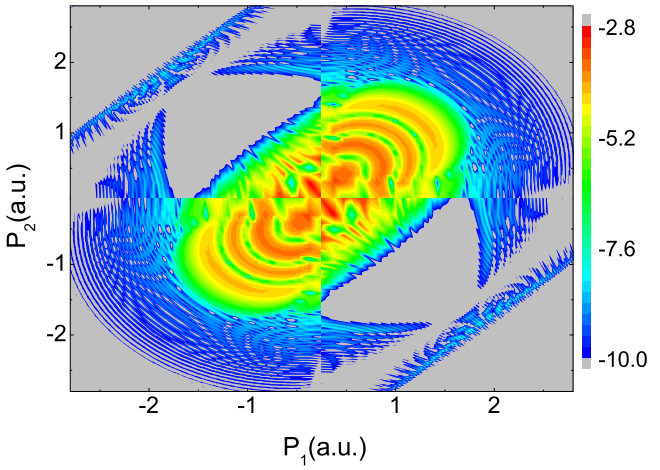

FIG. 1. The NSDI momentum spectra of two ionized electrons with their momenta parallel to the lasers polarization direction (on a logarithmic scale).

agrees with the result shown in Fig. 6 of Ref. [42], where the sideband pattern appears in the momentum or energy distribution that complies with energy conservation. One can see that the double ionization may happen when the two electron momenta are along the same or opposite directions, which is quite different from the case of the monochromatic IR laser [52]. Furthermore, the spectra in Fig. 1 demonstrate a two-plateau structure with complex patterns. In the following, we will explain how to form the multiplateau structure and where the interference pattern comes from.

As mentioned above, the NSDI can be treated as a two-step process, an ATI followed by an LAC. First, an electron is ionized by absorbing XUV and IR photons in the ATI process; then the ionized electron collides with the nucleus to make the two electrons ionize by absorbing or emitting more XUV or IR photons in the LAC process. According to previous work [15,16,18,53], we know that the XUV laser field plays a crucial role in the ionization process. First of all, the atom absorbs different numbers of XUV photons in the ATI process. Figure 2 shows the NSDI momentum spectra of the atom absorbing zero [Figs. 2(a1) and 2(b1)], one [Figs. 2(a2) and 2(b2)], and two [Figs. 2(a3) and 2(b3)] XUV photons in the ATI process. It is found that the process of absorbing one XUV photon dominates almost all contributions to the NSDI regardless of whether the momenta of the two ionized electrons are along the same [Figs. 2(a1)–2(a3)] or opposite [Figs. 2(b1)–2(b3)] directions, while the contributions of absorbing zero or two XUV photons can be neglected in the ATI process. This phenomenon can be easily understood: Since one XUV photon energy in our calculation is higher than the atomic double-ionization threshold, the ionization probability in the ATI step for the atom absorbing one XUV photon is much higher than other cases. Thus, the process of absorbing one XUV photon by the electron dominates the contribution to the NSDI, implying that the NSDI probability can be increased to a great extent by the XUV laser field, consistent with the result calculated by Hu [40].

In order to explain the structure of the NSDI spectra, we now define subchannels as (s_2, q_2), where s_2 and q_2 are, respectively,

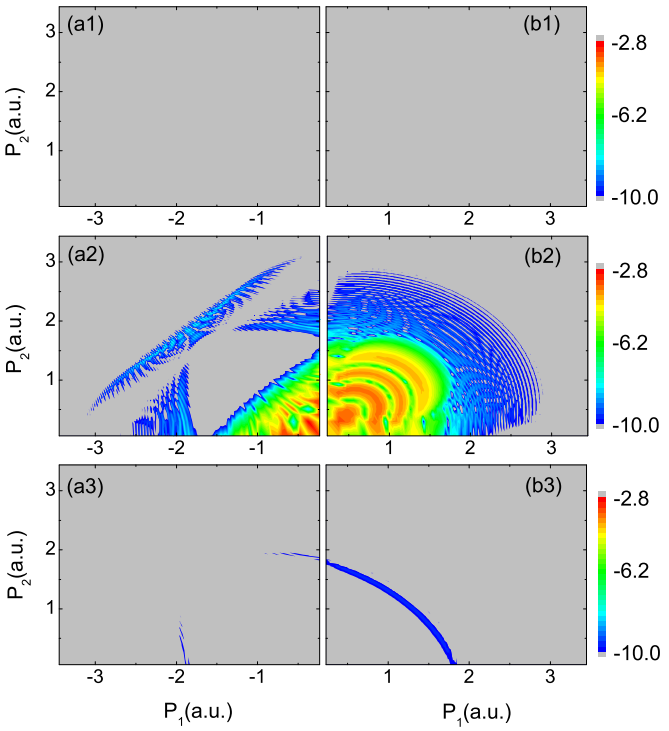

FIG. 2. The NSDI momentum spectra of the atom absorbing (a1) and (b1) zero, (a2) and (b2) one, and (a3) and (b3) two XUV photons in the ATI process (on a logarithmic scale).

the XUV photon numbers absorbed by the electrons in the ATI and LAC processes. Based on the results shown in Fig. 2, it is reasonable to set $s_2 = 1$. Figure 3 presents the channel contributions of the NSDI momentum spectra for two ionized

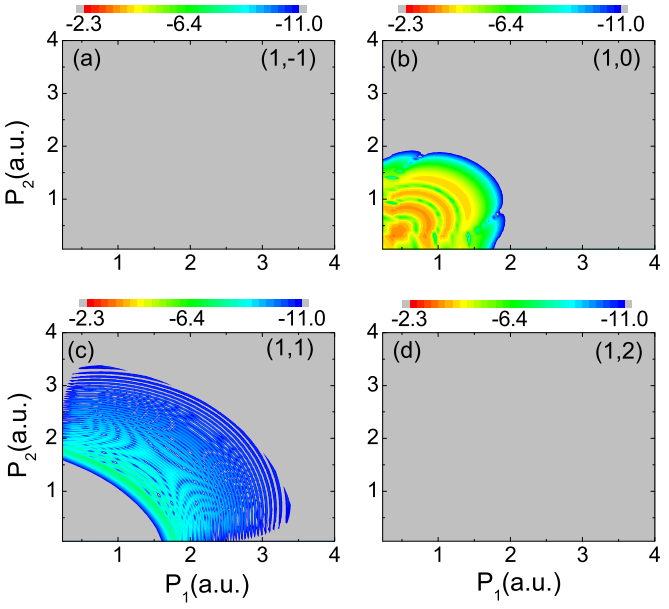

FIG. 3. Channel contributions of the NSDI momentum spectra of two ionized electrons with their momenta along the same direction for (a) $(1,-1)$, (b) $(1,0)$, (c) $(1,1)$, and (d) $(1,2)$ (on a logarithmic scale).

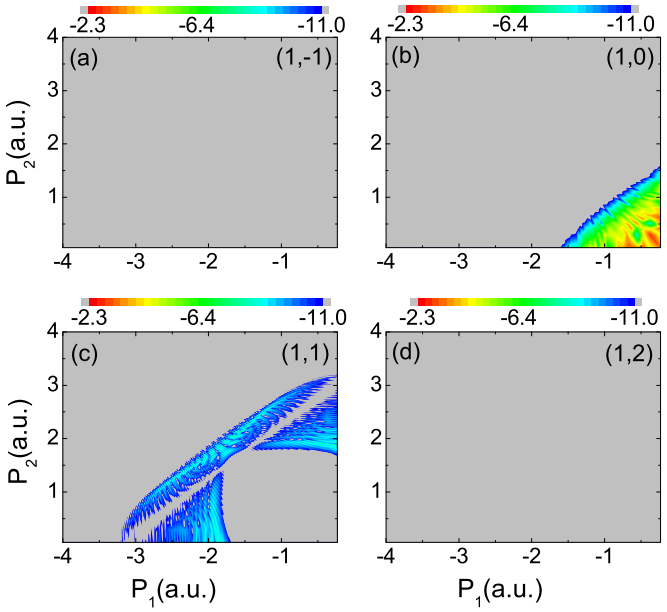

FIG. 4. Channel contributions of the NSDI momentum spectra of two ionized electrons with their momenta along the opposite directions for (a) (1,−1), (b) (1,0), (c) (1,1), and (d) (1,2) (on a logarithmic scale).

electrons with their momenta along the same direction for four subchannels (1,−1), (1,0), (1,1), and (1,2). One may find that the first and second plateaus shown in Fig. 2(b2) are from the contributions of subchannels (1,0) and (1,1), respectively. Comparing these two channels, one can see that if the ionized electron does not absorb the XUV photon during the LAC process, i.e., for the case of channel (1,0), the NSDI spectrum forms the first plateau; if the ionized electron absorbs another XUV photon during the LAC process, i.e., for the case of channel (1,1), the NSDI spectrum forms the second plateau. The probability of the first plateau is higher than that of the second plateau by about five orders of magnitude. Similarly, Fig. 4 shows channel contributions of the NSDI momentum spectra for two ionized electrons with their momenta along the opposite directions for four subchannels (1,−1), (1,0), (1,1), and (1,2). It is clear that the spectrum shown in Fig. 2(a2) comes from the summation of the contributions of subchannels (1,0) and (1,1), as shown in Figs. 4(b) and 4(c), respectively. Comparing Fig. 3 with Fig. 4, one may find that the plateau structure is quite different for the momenta of two ionized electrons along the same or opposite directions. We next focus on how to form the interference patterns of the two plateaus in the spectrum.

B. Forward and backward collisions

To explain the interference pattern shown in Figs. 3 and 4, we further define the subsubchannel (SSC) as $(s_2|s_1,q_2)$ in the subchannel (s_2,q_2), where s_1 is the number of IR photons that the electron absorbs ($s_1 > 0$) or emits ($s_1 < 0$) in an ATI process. According to our theory, since the NSDI is due to a collision process, the direction of the first ionized electron's momentum may be changed before and after the collision. In particular, if the angle between the momenta of the first ionized electron before and after the collision is smaller than $\pi/2$, we call this collision a forward collision; otherwise, if this angle is larger than $\pi/2$, we call the collision a backward collision.

We now consider the interference pattern of the first plateau shown in Fig. 3(b). Taking the SSCs of (1|−20,0), (1|0,0), (1|20,0), and (1|40,0) as examples, we present the NSDI momentum spectra for two ionized electrons with their momenta along the same direction in Figs. 5(a)–5(d). One can see that the kinetic energy increases and the ionization probability decreases with increasing s_1, which indicates that the more IR photons that the electron absorbs in the ATI process, the greater the final energy that the two electrons can carry after the collision and the lower the corresponding ionization probability is. To explain the interference pattern in more detail, we show the channel contributions of the NSDI momentum spectra with the forward collision in Figs. 5(e)–5(h) and the backward collision in Figs. 5(i)–5(l) for SSCs (1|−20,0) [Figs. 5(e) and 5(i)], (1|0,0) [Figs. 5(f) and 5(j)], (1|20,0) [Figs. 5(g) and 5(k)], and (1|40,0) [Figs. 5(h) and 5(l)]. Comparing Figs. 5(a)–5(d) with Figs. 5(e)–5(h) and Figs. 5(i)–5(l), one may find that the forward collision dominates the contributions to the NSDI process and the contributions of the backward collision decrease rapidly with the value of s_1 and are negligible for s_1 larger than zero. This can be understood as follows: When the ionized electron in the ATI process acquires more energy by absorbing the IR photons, it may have enough energy to trigger the second electron to ionize by a forward collision. Since the probability of the backward collision decreases with the kinetic energy of the incoming electron, the contributions of the backward collision to NSDI can be neglected for $s_1 > 0$. Comparing Fig. 3(b) with Figs. 5(a)–5(d), one can see that the interference pattern in Fig. 3(b) comes from the coherent summation over all the contributions from the SSCs.

Next we consider the interference pattern of the second plateau shown in Fig. 3(c) for $s_2 = 1$ and $q_2 = 1$. Taking the SSCs of (1|−20,1), (1|−10,1), (1|0,1), and (1|10,1) as examples, Figs. 6(a)–6(d) presents the NSDI momentum spectra of the two ionized electrons with their momenta along the same direction. Similar to the case of the subchannel (1,0) shown in Fig. 5, the kinetic energies of the electrons increase and the NSDI probability decreases as the IR photon number absorbed by the electron increases in the ATI process. Moreover, the forward collision here also plays a dominant role and the backward collision plays a negligible role in the NSDI process. We should note that the ionized electron absorbs another XUV photon when it collides with the other electron, which leads to a situation where the energy region of the second plateau in the NSDI spectrum is much larger than that of the first plateau.

On the other hand, the structure of the NSDI momentum spectra for two ionized electrons emitted in the opposite directions, as shown in Fig. 4, can also be explained by analyzing the contributions from different SSCs. Figure 7 presents the spectra of SSCs (1|−20,0), (1|0,0), (1|20,0), and (1|40,0) for the two ionized electrons with their momenta along the opposite directions. The spectra of the forward collisions are shown in Figs. 7(e)–7(h) and those of the backward collisions are shown in Figs. 7(i)–7(l). From Figs. 7(e)–7(h) and 7(i)–7(l) we may find that the kinetic energies of the electrons increase and the ionization probability decreases as the electron absorbs

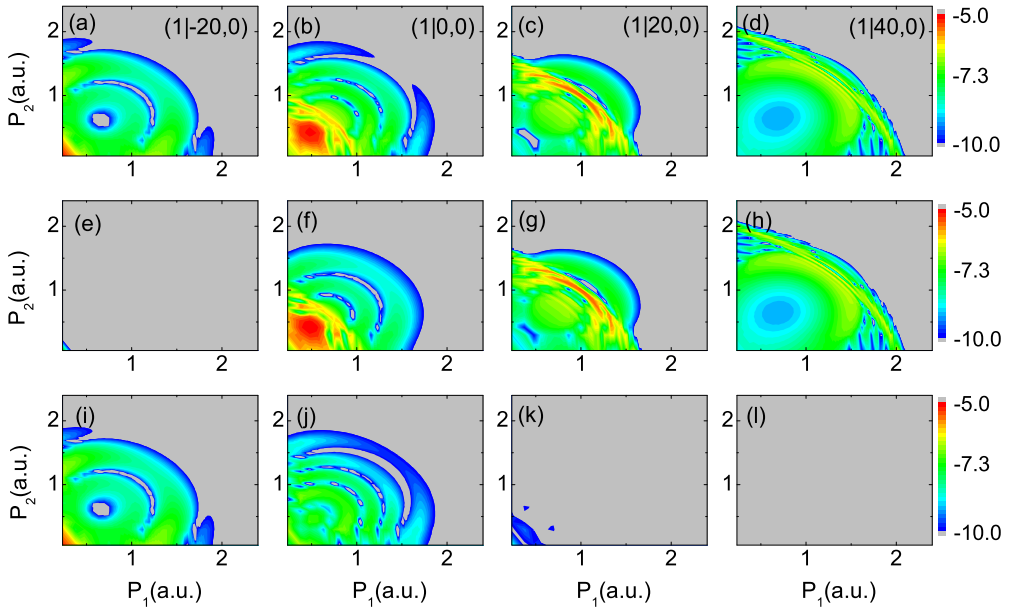

FIG. 5. Channel contributions of the NSDI momentum spectra of two ionized electrons with their momenta along the same direction for SSCs (a) (1|−20,0), (b) (1|0,0), (c) (1|20,0), and (d) (1|40,0). Also shown are the NSDI momentum spectra of the forward collision for SSCs (e) (1|−20,0), (f) (1|0,0), (g) (1|20,0), and (h) (1|40,0) and the NSDI momentum spectra of the backward collision for SSCs (i) (1|−20,0), (j) (1|0,0), (k) (1|20,0), and (l) (1|40,0) (on a logarithmic scale).

more IR photons in the ATI process. Furthermore, we find that both the forward and backward collisions now have comparable contributions to the NSDI spectrum, which is different from the case of Fig. 3, and their interference causes the basic interference patten of the first plateau in the NSDI spectrum shown in Fig. 4(b).

To understand the structure of the second plateau in the NSDI spectrum for the two ionized electrons with their momenta along opposite directions, as shown in Fig. 4(c), we show the subsubchannel spectra in Fig. 8 for SSCs (1|−20,1) [Figs. 8(a), 8(e), and 8(i)], (1|−10,1) [Figs. 8(b), 8(f), and 8(j)], (1|0,1) [Figs. 8(c), 8(g), and 8(k)], and (1|10,1) [Figs. 8(d), 8(h), and 8(l)], where the forward collision spectra are shown in Figs. 8(e)–8(h) and the backward collision spectra are shown in Figs. 8(i)–8(l). Similar to the first plateau, one may find that the forward and backward collisions make

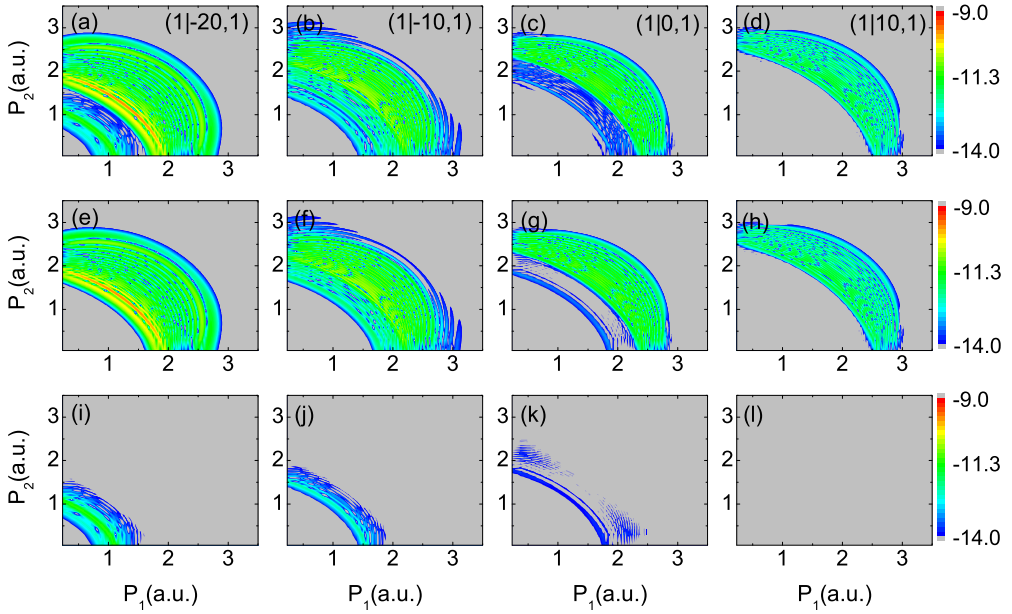

FIG. 6. Channel contributions of the NSDI momentum spectra of two ionized electrons with their momenta along the same direction for SSCs (a) (1|−20,1), (b) (1|−10,1), (c) (1|0,1), and (d) (1|10,1). Also shown are the NSDI momentum spectra of the forward collision for SSCs (e) (1|−20,1), (f) (1|−10,1), (g) (1|0,1), and (h) (1|10,1) and the NSDI momentum spectra of the backward collision for SSCs (i) (1|−20,1), (j) (1|−10,1), (k) (1|0,1), and (l) (1|10,1) (on a logarithmic scale).

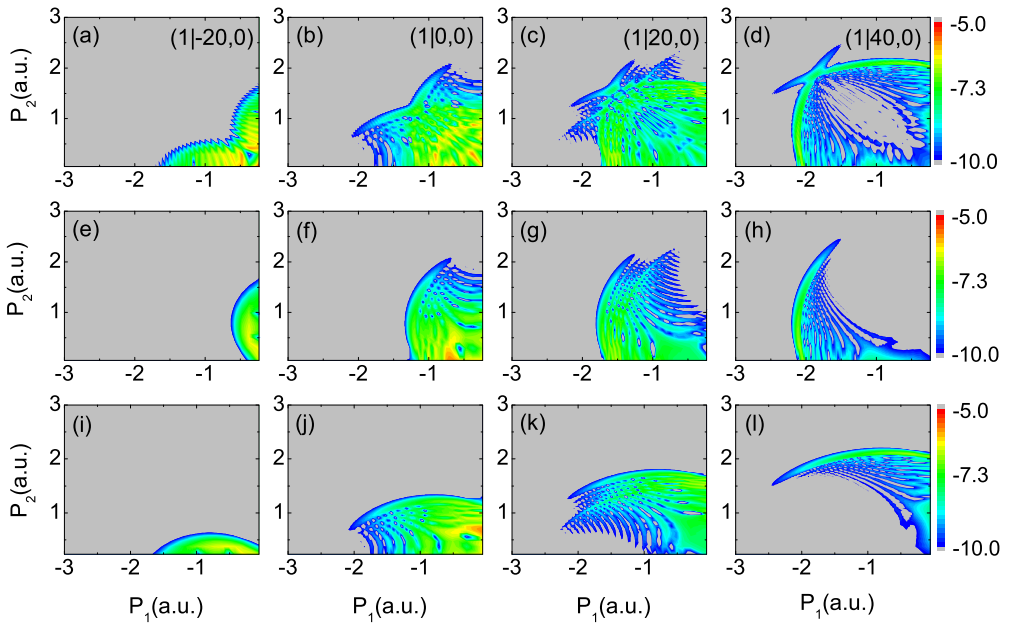

FIG. 7. Channel contributions of the NSDI momentum spectra of two ionized electrons with their momenta along the opposite directions for SSCs (a) (1|−20,0), (b) (1|0,0), (c) (1|20,0), and (d) (1|40,0). Also shown are the NSDI momentum spectra of the forward collision for SSCs (e) (1|−20,0), (f) (1|0,0), (g) (1|20,0), and (h) (1|40,0) and the NSDI momentum spectra of the backward collision for SSCs (i) (1|−20,0), (j) (1|0,0), (k) (1|20,0), and (l) (1|40,0) (on a logarithmic scale).

comparable contributions to the total NSDI probability and their interference causes the quantum interference structure of the second plateau in the NSDI spectrum as shown in Fig. 4(c). Comparing Figs. 8(e)–8(h) with Figs. 7(e)–7(h), we can see that the kinetic energy of the two electrons for SSC $(1|s_1,1)$ are higher than that for SSC $(1|s_1,0)$ with the same s_1 value, whereas the ionization probability of the spectrum for $(1|s_1,1)$ is smaller than that of the corresponding spectrum for $(1|s_1,0)$. These results come from the fact that the electron for subchannel $(1,1)$ absorbs one more XUV photon during the collision process.

C. Saddle-point approximation and energy circles

Let us consider the LAC process to explain the interference structure of the NSDI spectra of the SSCs shown in Figs. 5–8.

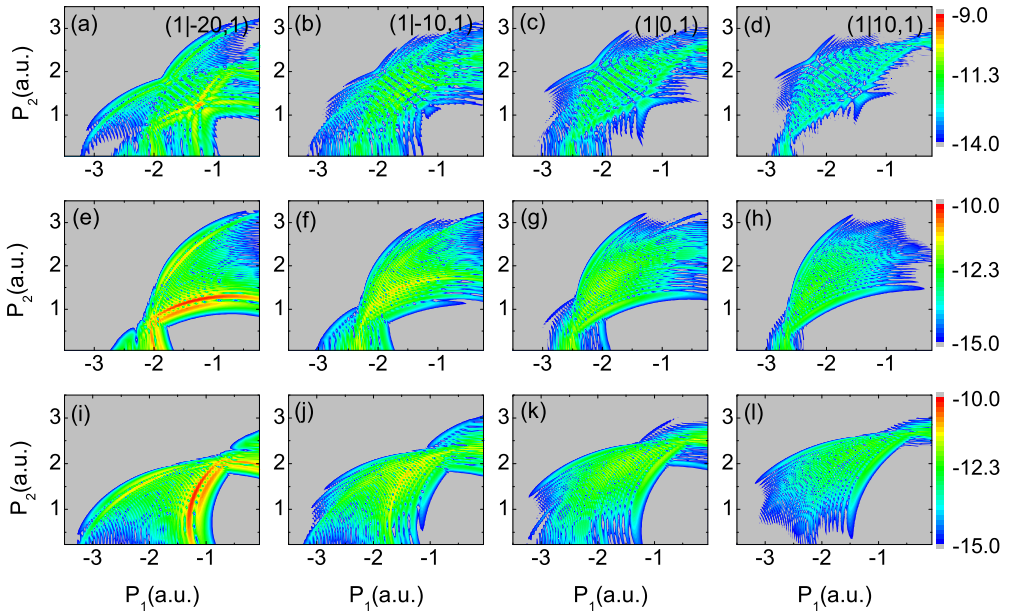

FIG. 8. Channel contributions of the NSDI momentum spectra of two ionized electrons with their momenta along the opposite directions for SSCs (a) (1|−20,1), (b) (1|−10,1), (c) (1|0,1), and (d) (1|10,1). Also shown are the NSDI momentum spectra of the forward collision for SSCs (e) (1|−20,1), (f) (1|−10,1), (g) (1|0,1), and (h) (1|10,1) and the NSDI momentum spectra of the backward collision for SSCs (i) (1|−20,1), (j) (1|−10,1), (k) (1|0,1), and (l) (1|10,1) (on a logarithmic scale).

We may analyze the LAC process by using the saddle-point approximation to the Bessel function $\aleph_{q_1q_2}(\zeta_1+\zeta_2-\zeta_1')$ in Eq. (10). The Bessel function can be simplified according to

$$\aleph_{q_1q_2}(\zeta_1+\zeta_2-\zeta_1') \approx J_{-q_1}(\zeta_{s1},\zeta_{s3})J_{-q_2}(\zeta_{s2}), \quad (12)$$

where

$$\begin{aligned}\zeta_{s1} &= 2\sqrt{\frac{u_{p_1}}{\omega_1}}|\mathbf{p}_1\cdot\hat{\varepsilon}_1+\mathbf{p}_2\cdot\hat{\varepsilon}_1-\mathbf{p}'\cdot\hat{\varepsilon}_1|,\\ \zeta_{s2} &= 2\sqrt{\frac{u_{p_2}}{\omega_2}}|\mathbf{p}_1\cdot\hat{\varepsilon}_2+\mathbf{p}_2\cdot\hat{\varepsilon}_2-\mathbf{p}'\cdot\hat{\varepsilon}_2|,\\ \zeta_{s3} &= \frac{1}{2}u_{p_1}.\end{aligned} \quad (13)$$

This Bessel function can be written in an integral form [46,50,53]

$$\begin{aligned}J_{-q_1}(\zeta_{s1},\zeta_{s3}) = \frac{1}{T_1}\int_{-T_1/2}^{T_1/2} dt\exp\{i[\zeta_{s1}\sin(\omega_1 t)\\ +\zeta_{s3}\sin(2\omega_1 t)+q_1\omega_1 t]\},\end{aligned} \quad (14)$$

where $T_1 = 2\pi/\omega_1$.

On the other hand, we can regard the IR laser field as a classical field, where the vector potential is $\mathbf{A}_{\rm cl}(t) = \hat{\varepsilon}_1 E_0/\omega_1\cos(\omega_1 t)$ with the amplitude of the laser's electric field E_0 and the polarization direction $\hat{\varepsilon}_1$. Therefore, the classical action of an electron in the IR laser field is

$$\begin{aligned}S_{\rm cl}(t,\mathbf{p}) &= \frac{1}{2}\int_0^t dt'[\mathbf{p}+e\mathbf{A}_{\rm cl}(t')]^2\\ &= \left(\frac{1}{2}\mathbf{p}^2+U_{p_1}\right)t+2\sqrt{\frac{u_{p_1}}{\omega_1}}|\mathbf{p}\cdot\hat{\varepsilon}_1|\sin(\omega_1 t)\\ &\quad+\frac{1}{2}u_{p_1}\sin(2\omega_1 t).\end{aligned} \quad (15)$$

Using the above classical action formula, the Bessel function can be rewritten as

$$J_{-q_1}(\zeta_{s1},\zeta_{s3}) = \frac{1}{T_1}\int_{-T_1/2}^{T_1/2} dt\exp\{i[\Delta S_{\rm cl}-(q_2\omega_2-I_{p_2})t]\}, \quad (16)$$

where $\Delta S_{\rm cl} \equiv S_{\rm cl}(t,\mathbf{p}_1)+S_{\rm cl}(t,\mathbf{p}_2)-S_{\rm cl}(t,\mathbf{p}')$. By applying the saddle-point approximation, Eq. (16) becomes

$$J_{-q_1}(\zeta_{s1},\zeta_{s3}) = 4\sqrt{\pi}/[T_1\sqrt{f''(t_0)}]\cos[f(t_0)-\pi/4], \quad (17)$$

where $f(t) \equiv \Delta S_{\rm cl}-(q_2\omega_2-I_{p_2})t$. The saddle point t_0 satisfies $f'(t_0)=0$, leading to the energy conservation relationship

$$\begin{aligned}&\tfrac{1}{2}\{[\mathbf{p}_1+e\mathbf{A}_{\rm cl}(t_0)]^2+[\mathbf{p}_2+e\mathbf{A}_{\rm cl}(t_0)]^2-[\mathbf{p}'+e\mathbf{A}_{\rm cl}(t_0)]^2\}\\ &\quad = q_2\omega_2-I_{p_2}.\end{aligned} \quad (18)$$

Hence we obtain the trajectories as

$$\begin{aligned}&[\mathbf{p}_1+e\mathbf{A}_{\rm cl}(t_0)]^2+[\mathbf{p}_2+e\mathbf{A}_{\rm cl}(t_0)]^2\\ &\quad = 2(q_2\omega_2-I_{p_2})+[\mathbf{p}'+e\mathbf{A}_{\rm cl}(t_0)]^2,\end{aligned} \quad (19)$$

where this equation can be regarded as the equation of the circle with its center $[-e\mathbf{A}_{\rm cl}(t_0),-e\mathbf{A}_{\rm cl}(t_0)]$ or $[-2\sqrt{U_{p1}}\cos(\omega_1 t_0),-2\sqrt{U_{p1}}\cos(\omega_1 t_0)]$ and the radius $R = \sqrt{2(q_2\omega_2-I_{p_2})+[\mathbf{p}'+e\mathbf{A}_{\rm cl}(t_0)]^2}$. Therefore, we may present the trajectories on the energy shell with a certain value of the saddle point t_0 and the momentum of the electron before collision $\mathbf{p}'$. In this paper, the LAC process can be treated as this process: The ionized electron with a certain momentum $\mathbf{p}'$ obtained from the ATI process collides with the parent ion, leading to the double ionization, where $|\mathbf{p}'| = \sqrt{2[(s_1+Ns_2)\omega_1-I_{p_1}-U_{p_1}-U_{p_2}]}$ with $N = \omega_2/\omega_1$. Hence, the photon numbers s_1 and s_2 in the ATI process determine the magnitude of momentum $\mathbf{p}'$. In our calculation, we set s_1 and s_2 equal to 0 and 1, respectively (if $s_2=1$ and $s_1=0$, $|\mathbf{p}'|$ corresponds to the mean value in the ATI process). Figures 9 and 10 present the SSC $(1|s_1,0)$ spectra for $\mathbf{p}'$ along the same (Fig. 9) and opposite (Fig. 10) direction of the laser's electric polarization, where the IR photon number is $s_1=0$. We may find that these energy circles agree well with the

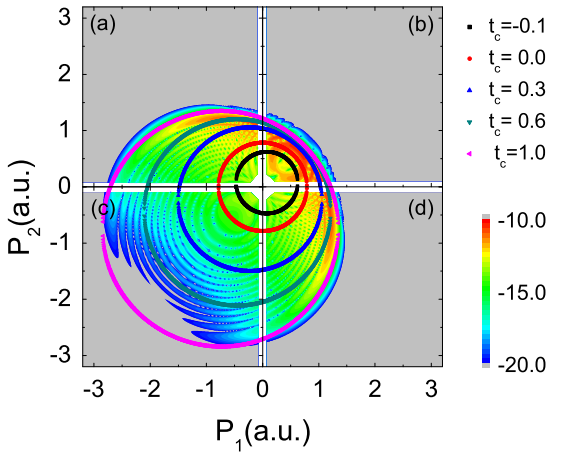

FIG. 9. The SSC $(1|s_1,0)$ spectra with $s_1=0$ and the corresponding energy circles at different collision moment $t_c=\cos(\omega_1 t_0)$ determined by Eq. (19) for $\mathbf{p}'$ along the same direction of the laser's electric polarization, which indicates that (b) and (d) are forward collisions and (a) and (c) are backward collisions (on a logarithmic scale).

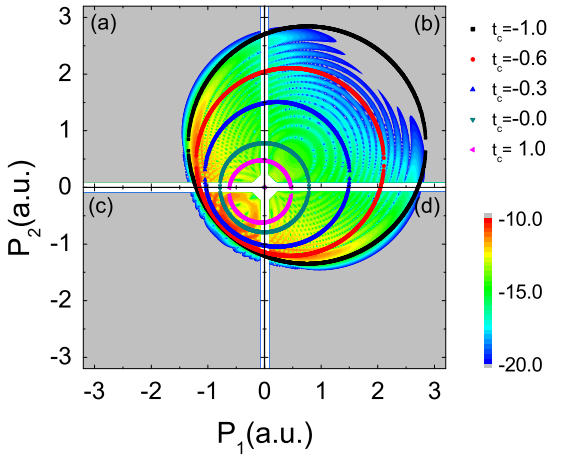

FIG. 10. The SSC $(1|s_1,0)$ spectra with $s_1=0$ and the corresponding energy circles at different collision moment $t_c=\cos(\omega_1 t_0)$ determined by Eq. (19) for $\mathbf{p}'$ along the opposite direction of the laser's electric polarization, which indicates that (b) and (d) are backward collisions and (a) and (c) are forward collisions (on a logarithmic scale).

numerical results and all the fringes in the NSDI spectrum come from the interference between the contributions from all the values of $\mathbf{p}'$. For the case of $\mathbf{p}_1$ and $\mathbf{p}_2$ along the same direction, we may find from Eq. (19) that the position of the circle center shifts along the line of $p_1 = p_2$ as the radius increases, and hence the orbits of the forward collision are limited in a relatively low energy region, while the orbits of the backward collision spread to a high energy region, as shown in Figs. 9(b) and 9(c) and also Figs. 10(b) and 10(c). As a result, the contribution of the forward collision to NSDI probability becomes larger than that of the backward collision, because the more photons that the electrons absorb, the lower the NSDI probability will be. On the other hand, for the case of $\mathbf{p}_1$ and $\mathbf{p}_2$ along opposite directions, as shown in Figs. 9(a), 9(d), 10(a), and 10(d), we may find that the forward and backward collisions make a comparable contribution to the NSDI because of the equivalent role of the two electrons. We should mention that the backward and forward collisions are subtly linked together by Eq. (19), which provides a different window to understand the structure of the first plateau in the NSDI spectrum: One electron is first ionized by absorbing one XUV photon and many IR photons and then it collides with the other electron with the assistance of the IR laser field, where the IR laser's electric field at the collision moment gives rise to the center and the radius of the energy circle.

For the case of subchannel (1,1), Figs. 11 and 12 show the SSC $(1|s_1,1)$ spectra for $\mathbf{p}'$ along the same (Fig. 11) and opposite (Fig. 12) direction of the laser's electric polarization, respectively, where the IR photon number is also $s_1 = 0$. Similarly, the energy circles agree well with quantum numerical results and the fringes in the NSDI spectra come from the interference between all these energy orbits. Same as the above case, the forward collision makes a dominant contribution to the NSDI probability for both electron momenta along the same direction, while the forward and backward collisions have comparable contributions to the NSDI probability. Comparing Fig. 12 with Fig. 10, one may find that the subchannel (1,1) dominates the higher energy region and forms the second plateau, since the ionized electron absorbs one more XUV photons during the collision.

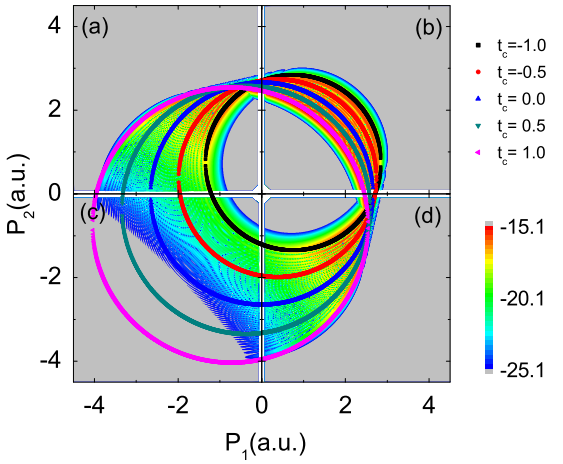

FIG. 11. The SSC $(1|s_1,1)$ spectra with $s_1 = 0$ and the corresponding energy circles at different collision moment $t_c = \cos(\omega_1 t_0)$ determined by Eq. (19) for $\mathbf{p}'$ along the same direction of the laser's electric polarization, which indicates that (b) and (d) are forward collisions and (a) and (c) are backward collisions (on a logarithmic scale).

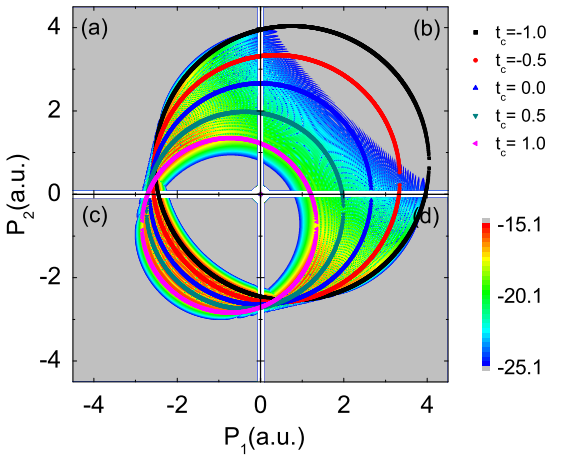

FIG. 12. The SSC $(1|s_1,1)$ spectra with $s_1 = 0$ and the corresponding energy circles at different collision moment $t_c = \cos(\omega_1 t_0)$ determined by Eq. (19) for $\mathbf{p}'$ along the opposite direction of the laser's electric polarization, which indicates that (b) and (d) are backward collisions and (a) and (c) are forward collisions (on a logarithmic scale).

Furthermore, by using the channel analysis, we may find that the interference patterns in Fig. 1 are due to the contributions of each ATI channel of collision. From the saddle-point approximation (17), we can find that the interference pattern comes from the function $\cos[f(t_0) - \pi/4]$, which is from the interference term at the collision moment t_0 and $2\pi/\omega_1 - t_0$. When the function $\cos[f(t_0) - \pi/4]$ is zero, the destructive interference appears, as shown by the closed squares in Figs. 13(a) and 13(b) for the SSC (1|20,0) and in Figs. 14(a) and 14(b) for the SSC $(1|-10,1)$. One may see that the distribution of the dark squares agrees with the locations of the destructive interference fringes by the numerical calculation, which indicates that the interference pattern comes from the interference of the trajectories at different saddle points t_0 and $2\pi/\omega_1 - t_0$ when the collision happens.

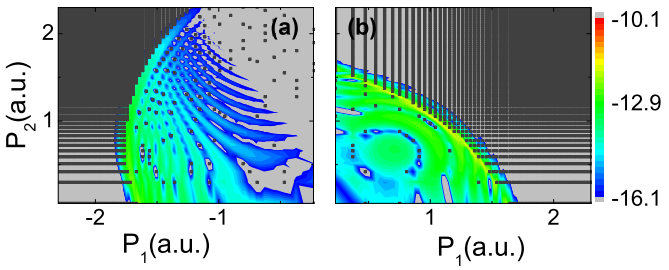

FIG. 13. Interference pattern on the NSDI momentum distributions of SSC (1|20,0) for the forward collision of two ionized electrons with their momenta along (a) the opposite directions and (b) the same direction. The closed squares are the locations of destructive interference determined by $\cos[f(t_0) - \pi/4] = 0$ in Eq. (17) (on a logarithmic scale).

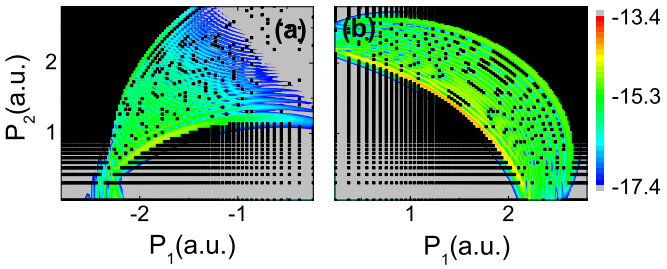

FIG. 14. Interference pattern on the NSDI momentum distributions of SSC $(1|-10,1)$ for the forward collision of two ionized electrons with their momenta along (a) the opposite directions and (b) the same direction. The closed squares are the locations of destructive interference determined by $\cos[f(t_0) - \pi/4] = 0$ in Eq. (17) (on a logarithmic scale).

IV. CONCLUSION

We have investigated the NSDI process caused by the CI mechanism in a combined IR+XUV two-color laser field, where the XUV photon energy is higher than the ionization threshold. The NSDI momentum spectra show a multiplateau structure. By applying the channel analysis, the height of the plateau is determined by the number of XUV photons absorbed by the electrons. Furthermore, we have considered the contributions from the forward and backward collisions to the NSDI probability. We have found that when the momenta of the two ionized electrons are along the same direction, the forward collision dominates the contributions to the NSDI probability; when the momenta of the two ionized electrons are along the opposite directions, the forward and backward collisions make a comparable contribution to the NSDI probability. By applying the saddle-point approximation, we have obtained a classical energy formula covering the forward and backward collisions, which opens a possibility to understand the interference pattern in momentum spectra. Moreover, it has been found that the interference pattern of the NSDI momentum spectrum is from the coherent summation over the contributions of all ATI channels and is also attributed to the interference between two trajectories born at different saddle points t_0 and $2\pi/\omega_1 - t_0$ when the collision happens in each channel.

ACKNOWLEDGMENTS

This research was supported by the National Natural Science Foundation of China under Grants No. 11474348 and No. 61275128. Z.-C.Y. was supported by the Natural Sciences and Engineering Research Council of Canada and by the Canadian computing facilities of SHARCnet, and ACEnet.

[1] C. Liu and T. Nakajima, Phys. Rev. A **78**, 063424 (2008).
[2] C. Liu, T. Nakajima, T. Sakka, and H. Ohgaki, Phys. Rev. A **77**, 043411 (2008).
[3] H. Eichmann, A. Egbert, S. Nolte, C. Momma, B. Wellegehausen, W. Becker, S. Long, and J. K. McIver, Phys. Rev. A **51**, R3414 (1995).
[4] I. J. Kim, C. M. Kim, H. T. Kim, G. H. Lee, Y. S. Lee, J. Y. Park, D. J. Cho, and C. H. Nam, Phys. Rev. Lett. **94**, 243901 (2005).
[5] S. Watanabe, K. Kondo, Y. Nabekawa, A. Sagisaka, and Y. Kobayashi, Phys. Rev. Lett. **73**, 2692 (1994).
[6] C. F. de Morisson Faria, M. Dörr, W. Becker, and W. Sandner, Phys. Rev. A **60**, 1377 (1999).
[7] C.-L. Xia and X.-S. Liu, Phys. Rev. A **87**, 043406 (2013).
[8] X. Wang, C. Jin, and C. D. Lin, Phys. Rev. A **90**, 023416 (2014).
[9] X. Cao, S. Jiang, C. Yu, Y. Wang, L. Bai, and R. Lu, Opt. Express **22**, 26153 (2014).
[10] X.-L. Ge, H. Du, J. Guo, and X.-S. Liu, Opt. Express **23**, 8837 (2015).
[11] I.-L. Liu, P.-C. Li, and S.-I. Chu, Phys. Rev. A **84**, 033414 (2011).
[12] Y. Chou, P.-C. Li, T.-S. Ho, and S.-I. Chu, Phys. Rev. A **91**, 063408 (2015).
[13] L. Zhang, X. Xie, S. Roither, Y. Zhou, P. Lu, D. Kartashov, M. Schöffler, D. Shafir, P. B. Corkum, A. Baltuška, A. Staudte, and M. Kitzler, Phys. Rev. Lett. **112**, 193002 (2014).
[14] M. Richter, M. Kunitski, M. Schöffler, T. Jahnke, L. P. H. Schmidt, M. Li, Y. Liu, and R. Dörner, Phys. Rev. Lett. **114**, 143001 (2015); Z. Yuan, D. Ye, Q. Xia, J. Liu, and L. Fu, Phys. Rev. A **91**, 063417 (2015).
[15] K. Zhang, J. Chen, X.-L. Hao, P. Fu, Z.-C. Yan, and B. Wang, Phys. Rev. A **88**, 043435 (2013).
[16] P. Radcliffe, M. Arbeiter, W. B. Li, S. Düsterer, H. Redlin, P. Hayden, P. Hough, V. Richardson, J. T. Costello, T. Fennel, and M. Meyer, New J. Phys. **14**, 043008 (2012).
[17] V. Véniard, R. Taïeb, and A. Maquet, Phys. Rev. Lett. **74**, 4161 (1995).
[18] A. K. Kazansky, I. P. Sazhina, and N. M. Kabachnik, Phys. Rev. A **86**, 033404 (2012); J. Phys. B **46**, 025601 (2013).
[19] A. l'Huillier, L. A. Lompre, G. Mainfray, and C. Manus, Phys. Rev. A **27**, 2503 (1983).
[20] B. Walker, B. Sheehy, L. F. DiMauro, P. Agostini, K. J. Schafer, and K. C. Kulander, Phys. Rev. Lett. **73**, 1227 (1994).
[21] R. Kopold, W. Becker, H. Rottke, and W. Sandner, Phys. Rev. Lett. **85**, 3781 (2000).
[22] T. Weber, M. Weckenbrock, A. Staudte, L. Spielberger, O. Jagutzki, V. Mergel, F. Afaneh, G. Urbasch, M. Vollmer, H. Giessen, and R. Dörner, Phys. Rev. Lett. **84**, 443 (2000).
[23] J. Chen, J. Liu, and W. M. Zheng, Phys. Rev. A **66**, 043410 (2002); J. Chen and C. H. Nam, *ibid.* **66**, 053415 (2002); J. Chen, J. Liu, L. B. Fu, and W. M. Zheng, *ibid.* **63**, 011404(R) (2000).
[24] Y. Liu, S. Tschuch, A. Rudenko, M. Dürr, M. Siegel, U. Morgner, R. Moshammer, and J. Ullrich, Phys. Rev. Lett. **101**, 053001 (2008).
[25] P. B. Corkum, Phys. Rev. Lett. **71**, 1994 (1993).
[26] W. Becker, X. Liu, P. J. Ho, and J. H. Eberly, Rev. Mod. Phys. **84**, 1011 (2012), and references therein.

[27] H. Li, J. Chen, H. Jiang, J. Liu, P. Fu, Q. Gong, Z.-C. Yan, and B. Wang, J. Phys. B **42**, 125601 (2009).
[28] A. Becker and F. H. M. Faisal, Phys. Rev. Lett. **89**, 193003 (2002).
[29] D. F. Ye, X. Liu, and J. Liu, Phys. Rev. Lett. **101**, 233003 (2008).
[30] J. S. Briggs and V. Schmidt, J. Phys. B **33**, R1 (2000).
[31] M. S. Schöffler, C. Stuck, M. Waitz, F. Trinter, T. Jahnke, U. Lenz, M. Jones, A. Belkacem, A. L. Landers, M. S. Pindzola, C. L. Cocke, J. Colgan, A. Kheifets, I. Bray, H. Schmidt-Böcking, R. Dörner, and T. Weber, Phys. Rev. Lett. **111**, 013003 (2013).
[32] Y. Nabekawa, H. Hasegawa, E. J. Takahashi, and K. Midorikawa, Phys. Rev. Lett. **94**, 043001 (2005).
[33] A. A. Sorokin, M. Wellhöfer, S. V. Bobashev, K. Tiedtke, and M. Richter, Phys. Rev. A **75**, 051402(R) (2007).
[34] A. Rudenko *et al.*, Phys. Rev. Lett. **101**, 073003 (2008).
[35] L.-Y. Peng, W.-C. Jiang, J.-W. Geng, W.-H. Xiong, and Q. Gong, Phys. Rep. **575**, 1 (2015).
[36] A. Liu and U. Thumm, Phys. Rev. Lett. **115**, 183002 (2015).
[37] X. Guan, K. Bartschat, and B. I. Schneider, Phys. Rev. A **77**, 043421 (2008).
[38] A. Palacios, T. N. Rescigno, and C. W. McCurdy, Phys. Rev. A **79**, 033402 (2009).
[39] B. Kaiser, A. Vagov, V. M. Axt, and U. Pietsch, Phys. Rev. A **84**, 043431 (2011).
[40] S. X. Hu, Phys. Rev. Lett. **111**, 123003 (2013).
[41] A. Liu and U. Thumm, Phys. Rev. A **91**, 043416 (2015).
[42] A. Liu and U. Thumm, Phys. Rev. A **89**, 063423 (2014).
[43] M. Gell-Mann and M. L. Goldberger, Phys. Rev. **91**, 398 (1953); M. L. Goldberger and K. M. Watson, *Collision Theory* (Wiley, New York, 1964).
[44] D.-S. Guo and G. W. F. Drake, J. Phys. A: Math. Gen. **25**, 5377 (1992).
[45] L. Gao, X. Li, P. Fu, R. R. Freeman, and D.-S. Guo, Phys. Rev. A **61**, 063407 (2000).
[46] B. Wang, L. Gao, X. Li, D.-S. Guo, and P. Fu, Phys. Rev. A **75**, 063419 (2007).
[47] H. Kang, W. Quan, Y. Wang, Z. Lin, M. Wu, H. Liu, X. Liu, B. B. Wang, H. J. Liu, Y. Q. Gu, X. Y. Jia, J. Liu, J. Chen, and Y. Cheng, Phys. Rev. Lett. **104**, 203001 (2010).
[48] P. Fu, B. Wang, X. Li, and L. Gao, Phys. Rev. A **64**, 063401 (2001).
[49] T. Cheng, X. Li, S. Ao, L.-A. Wu, and P. Fu, Phys. Rev. A **68**, 033411 (2003).
[50] Y. Guo, P. Fu, Z.-C. Yan, J. Gong, and B. Wang, Phys. Rev. A **80**, 063408 (2009).
[51] B. Wang, Y. Guo, B. Zhang, Z. Zhao, Z.-C. Yan, and P. Fu, Phys. Rev. A **82**, 043402 (2010).
[52] B. Wang, Y. Guo, J. Chen, Z.-C. Yan, and P. Fu, Phys. Rev. A **85**, 023402 (2012).
[53] M. Liu, Y. Guo, Z.-C. Yan, and B. Wang, Chin. Phys. B **24**, 073201 (2015).